

# Postprint

Version définitive du manuscrit publié dans / Final version of the manuscript published in : **LAGOUARDE J.-P., IRVINE M. Directional anisotropy in thermal infrared measurements over Toulouse city centre during the CAPITOUL measurement campaigns: first results. Meteorology and Atmospheric Physics, numéro spécial CAPITOUL. 19 p.**

**Directional anisotropy in thermal infrared measurements over Toulouse city centre during the CAPITOUL measurement campaigns : first results**

J-P. Lagouarde, M. Irvine

*INRA, UR1263 EPHYSE, 71 avenue E. Bourlaux, F-33140 Villenave d'Ornon, France*

*ABSTRACT. The measurements of surface temperature are prone to important directional anisotropy related to the structure of the canopy and the radiative and energy exchanges inside of it. Directional effects must be taken into account for a number of practical applications such as the correction of large swath satellite data, the assimilation of thermal infrared (TIR) measurements in surface models, the design of future spatial missions... For urban canopies, experimental measurements of TIR directional anisotropy previously performed during summer days over Marseille in the framework of the ESCOMPTE campaign (2001) revealed significant angular surface temperature variations with noticeable hot spot effects whose intensity was related to the canopy structure. The CAPITOUL project (<http://medias.cnrs.fr/capitoul/>) provided the opportunity to extend these results to other seasons and to nighttime conditions. The experimental setup is based on the use of 2 airborne TIR cameras with different lenses, inclination and resolution, and installed aboard a small aircraft. The flight protocol allowed the retrieval of directional anisotropy in all azimuthal directions and in a range of zenith viewing angles between nadir and 62°. Measurements were performed during several intensive operation periods (IOP) in summer (2004 July), autumn (2004 September and October) and winter (2005 February). Only the first results of the 2004 autumn and 2005 winter IOPs are presented in this paper. The results obtained in daytime conditions confirm the systematic hot spot effects observed in previous experiments over cities. The variations found seem to be particularly important in winter when sun elevation is low: for instance they range between -4 and 10K between oblique and nadir viewing in February. During nighttime conditions, angular variations are much lower (always less than 2K between nadir and 60° zenithal viewing angle), whichever the azimuthal viewing direction.*

## 1 INTRODUCTION

As the surface temperature is tightly related to the energy budget of canopies, remote sensing in the thermal infrared (TIR) provides a valuable source of data for studying urban climates (Arnfield, 2003, Voogt & Oke, 2003). For instance, series of satellite TIR imagery have been used to analyse the possible impact of urbanization on climate warming (Owen et al., 1998). TIR data have also been used to map and evaluate the intensity of urban heat islands (Roth et al., 1989, Streukler, 2003). The increasing attention paid over the last years to air pollution and air quality in cities has led to the development of a number of numerical models to simulate dynamics and thermodynamics of the urban atmosphere (Grimmond & Oke, 2002, Masson, 2000, Martilli et al., 2002, Voogt & Grimmond, 2000) in which the surface temperature appears as an important variable. Some of them are based on simplified ‘canyon street’ schemes (Masson, 2000 ; Martilli et al., 2001), others on explicit description

of the 3D structure of the urban canopies (SUM by Soux et al., 2000, SOLENE by Vinet, 2000, DARTEB by Gastellu et al., 2004 and Guillevic et al., 2003). Coupled radiative and energy transfers inside urban canopies depend on canopy structure and induce shadowing effects and large temperature variability across the different facets resulting in potentially important TIR directional anisotropy at larger scales (Voogt & Oke, 1997 and 1998; Wang et al., 2001). This must be properly considered to allow progress in the description of the urban climates such as the assessment of non-biased estimations of surface heat fluxes (Vogt & Oke, 1997) or longwave upward radiation flux (Sugawara & Takamura, 2006), and the characterization of urban heat island intensity. A review can be found in Voogt and Oke (2003). The TIR anisotropy must also be considered when using large swath satellite data for which zenith viewing angles may reach important values, up to  $\pm 57^\circ$  for the AVHRR sensor for instance.

Experimental campaigns have been performed to assess TIR anisotropy and to collect validation data sets. Lagouarde et al. (2004) describe a methodology based on the use of airborne TIR camera and present results obtained in daytime summer conditions over the city of Marseille (France) which revealed important hot spot effects. The CAPITOUL project (<http://medias.cnrs.fr/capitoul/>) conducted over the city of Toulouse provided the opportunity to study the cases of nighttime and winter conditions and winter which are less documented up to now. Results obtained during the 2004 autumn and 2005 winter intensive observation periods are presented in this paper.

## 2 DEFINITIONS

The skin temperature of any element (vegetal, soil, urban facets...) within a canopy is governed by coupled energy (heat and water fluxes) and radiative transfers (emission and reflection of the surrounding ambient radiation); it depends on a number of parameters among which the structure of the canopy and the surface radiative properties play major roles. The overall energy, as measured in a given direction by a TIR sensor placed close to the surface, results from the integration, in the spectral windows of the instrument, of the TIR radiation coming from all the facets of the canopy 'seen' in the FOV. We define the brightness surface temperature as the black body temperature that would provide the same measurement.

If an overall emissivity value -or 'ensemble emissivity' as defined by Becker & Li, 1995- is introduced, a surface radiative temperature -or 'radiometric temperature' as defined by Norman & Becker, 1995- of the canopy can be estimated provided that the ambient radiation is known. Because it includes 'cavity effects' and multiple reflection effects (Sutherland and Bartholic, 1977; François & al., 1997), it is difficult to define an unequivocal value of 'effective emissivity', and the temperature emissivity separation remains a difficult problem. Assumptions on emissivity must therefore be made. One consists in assuming the emissivity to be lambertian with a uniform value (no spectral dependency). Contrary to other authors who propose to condense all the angular dependence into emissivity with no angular variations on the retrieved surface temperature (Li et al., 1999), this comes to condense all the angular dependency into the radiometric temperature. If the emissivity is set to 1, the corresponding radiative temperature is equivalent to the brightness surface temperature. In this paper the emissivity of the urban canopy will be assumed to be lambertian and will be given an arbitrary but realistic value of 0.95, the surface temperature derived from airborne measurements therefore being a surface radiometric temperature. The reader is referred to the paper of Lagouarde et al. (2004) for more details regarding its definition.

## 3 EXPERIMENTAL

### 3.1 Observational setup and flight protocol

The TIR measurements were performed using 2 airborne TIR cameras placed aboard a small twin-engine aircraft Piper Aztec PA23 flown by SAFIRE group (<http://www.safire.fr/> Service des Avions Français Instrumentés pour la Recherche en Environnement). The 2 cameras INFRAMETRICS M740 and FLIR SC2000<sup>(1)</sup> were equipped with 75.2° x 58.7° wide angle and 23.8° x 17.9° FOV lenses respectively and placed aboard the aircraft with backward inclinations of 9.5 and 50° (Figure 1), thus resulting in a partial overlapping of their FOV which allowed to intercalibrate the two instruments (see further). The aircraft speed was 70 ms<sup>-1</sup>; acquisition rates of images were 1 and 4.3 Hz respectively. Initially chosen at 1500ft for the first flights, the flight height was then increased to 1800-2000ft to have a larger ground image aimed at and a better integration of the surface heterogeneity. The spatial resolutions ranged between 2.5 m (nadir) and 6.2 m (50° zenith viewing) for M740 and between 1.5 and 3.0 m for SC2000 (for 48 and 62° zenith viewing angles respectively). An additional filter was mounted on the SC2000 to eliminate too important atmospheric contribution in the measured signal above 13µm and to make the spectral windows of both cameras nearly similar and comprised between 7.5 and 13 µm.

The protocol of measurements consists of several short flight lines flown in different directions all crossing at the city centre. Flying successive flight lines in opposite directions allows one to observe the surface below with up to ±47° angles along track within a short time interval with the M740 instrument (Fig.1). Combining with the SC2000 data extends the range of zenithal viewing angles up to 62°. For daytime measurements, the direction of the flight lines is imposed by the sun position (i.e. the time) with the first line flown in the principal plane and facing the sun (Fig. 2). The second flight axis allows one to study the variations of the surface temperature within the perpendicular plane. Finally the flight protocol includes 2 additional lines flown in directions ±45° from the principal plane. For nighttime, no particular direction is privileged, and the 4 flown axis are N↔S, W↔E, NW↔SE and NE↔SW. As every point of the obtained images corresponds to a particular configuration of azimuth and zenith viewing angles, the combination of the different flight segments allows one to retrieve the TIR directional anisotropy for all azimuthal directions and for zenith viewing angles up to 50° (and possibly 62° when using both cameras), so making useless any gap-filling when processing the data. For more details, the reader is referred to previous papers (Lagouarde et al., 2000 and 2004).

### 3.2 Experimental site and dataset

The urban city centre of Toulouse (about 2x3 km) is densely built with narrow streets in all directions and no vegetation (Fig.3).

Most buildings are old and the materials most commonly used are brick for walls and tiles for roofs. A central site equipped for continuous monitoring of the urban surface layer (measurements of surface fluxes, radiation budget...) was situated close to the Capitole square (Masson et al., 2007). In its vicinity, the mean height of walls is about 15m. The other characteristic ratios relative to the plan area are 0.54 (roofs), 0.38 (roads), 0.08 (vegetation) and 1.3 (walls). By interpreting air photos a homogeneous area representative of the city centre was delimited from which TIR anisotropy was extracted from.

---

<sup>(1)</sup> Trade name and company are given for the benefit of the reader and do not imply any endorsement of the product or company by the authors.

TIR airborne measurements were performed during several intensive operation periods (IOP) in 2004 and 2005. In this paper we focus on autumn (2004 October IOP) and winter (2005 February IOP) conditions for which anthropogenic effects (heating of buildings) are expected to have more impact (Pigeon et al., 2006). 6 flights, 3 in nighttime and 3 in daytime conditions (morning and afternoon) are analysed for comparison purposes (Table 1). The flight times were chosen around 10:00 or 11:00 UT mid morning long enough after sunrise to have a heating impact by the sun, and around 14:00 mid afternoon when surface temperature is close to its maximum value. The quality of the October 4<sup>th</sup> afternoon flight is bad and it has not been processed. For nighttime the measurements times were chosen around 22:00 and 23:00 UT late enough to ensure prevailing radiative cooling without any residual inertia effect of the previous day, and early enough to avoid possible development of fog close to the surface.

### 3.3 Data processing

Several calibration tests of the cameras had previously been performed at the laboratory by aiming at a water surface in a thermo-regulated bath: they revealed that the SC2000 calibration curve is stable with time and consistent with the technical specifications provided by the manufacturer (Fig. 4). The calibration of the M740 camera is less satisfactory because it exhibits a lack of temporal stability over long periods and sensitivity to its internal temperature. The calibration of this instrument was therefore adjusted afterwards during the processing of data by comparison against the SC2000 camera considered as the reference, using the overlapping area between images (Fig. 5). We are unable to explain the fact - already observed with this instrument in previous experiments- that the intercept appears to be very far from zero in Fig. 5. As the spectral windows of the 2 cameras are slightly different, the impact of the atmospheric effects in the simultaneous measurements they provide may slightly differ; this was taken into account in this intercalibration process, using the LOWTRAN 7 model to remove the contribution of the atmosphere.

The same model was also used to correct for the atmospheric effects  $\delta_{\text{atm}}$  and to retrieve actual surface radiometric temperatures  $T_s$  from the measured brightness temperature at the aircraft level  $T_{b_{\text{meas}}}$ :  $T_s = T_{b_{\text{meas}}} + \delta_{\text{atm}}$ . Radiosoundings performed by Météo France close to the centre of the city simultaneously with the flights provided the atmospheric profiles of temperature and humidity. The atmospheric transmittances at 10  $\mu\text{m}$  and averaged over the spectral window 7.5 – 13  $\mu\text{m}$  of the cameras provide an order of magnitude of the atmospheric turbidity : for the February flights they are quite similar and range between 0.952 and 0.964 at 10  $\mu\text{m}$  and between 0.976 and 0.981 for the averaged values. For the autumn flights, the atmosphere appears to be more turbid with values 0.922 / 0.900 at 10  $\mu\text{m}$  and 0.839 / 0.804 for flights 0441 / 0443 respectively. The contribution of atmospheric effects, which depend on the zenithal viewing angle which in turn determines the optical path, must be removed in order to extract the directional anisotropy related to the structure of the canopy itself. The angular variation of atmospheric corrections may be significant as illustrated in Fig 6 and 7, where the atmospheric angular contribution is plotted against the zenithal viewing angle for flights 0441 (daytime) and 0510 (nighttime). The atmospheric angular contribution is the difference between the atmospheric correction at a given viewing angle and the atmospheric correction at nadir  $\delta_{\text{atm}}(\theta_v) - \delta_{\text{atm}}(0)$  for a given surface temperature  $T_s$  (with  $\delta_{\text{atm}}(\theta_v) = T_s - T_{\text{LOW7}}(\theta_v)$ ,  $\delta_{\text{atm}}(0) = T_s - T_{\text{LOW7}}(0)$ ,  $T_{\text{LOW7}}(\theta_v)$  being the temperature computed by LOWTRAN7 at the sensor level); it therefore represents the impact of the atmosphere itself in the measured directional surface temperature. After these corrections, the temperature finally retrieved from the airborne measurements is a radiative (or ‘radiometric’) surface temperature.

Geometric (barrel-type deformations) and radiometric distortions (non-homogeneities in the images, principally affecting the corners) related to the use of the 76° M740 wide angle lenses were also analysed and corrected (Lagouarde et al., 2004).

Details about the computation of zenithal ( $\theta_v$ ) and azimuthal ( $\varphi_v$ ) viewing angles and the characterisation of directional anisotropy are found in Lagouarde et al. (2000 and 2004). Here we only state the main steps. For each flight line, an average nadir temperature is computed from M740 data and a series of values of directional anisotropy  $\Delta T_s = T_{S_{\text{off nadir}}} - T_{S_{\text{nadir}}}$  (oblique minus nadir temperatures) for every ( $\theta_v, \varphi_v$ ) is extracted from the images over the area of interest, and stored. After the analysis of all the flight lines an average value of  $\Delta T_s$  is computed for every ( $\theta_v, \varphi_v$ ) and a final matrix (with rows and columns corresponding to  $\theta_v$  and  $\varphi_v$  binned into 1° classes respectively) containing the resulting averaged  $\Delta T_s$  is generated. In addition to this, the standard deviation ( $\sigma$ ) and the number of measurements ( $n$ ) used in the averaging are calculated. This makes possible the estimation of a  $\Delta T_s$  confidence interval, i.e.  $2\sigma/n^{1/2}$ . An additional advantage of the current method is that the mixing of measurements from different locations and different times for every view angle naturally results in a ‘spatio-temporal’ smoothing of the  $\Delta T_s$  values. In this paper, we neglected to correct for pitch and roll angles. Despite the stability of the aircraft being excellent, this could induce errors estimated to be about  $\pm 3^\circ$  in  $\theta_v$  and  $\varphi_v$  angles.

The sensitivity to the emissivity  $\varepsilon$  around the 0.95 value, that was assumed, has been tested. As expected, computations made with  $\varepsilon = 0.90$  and  $\varepsilon = 1.0$  revealed an important impact (several K) on the absolute retrieved values of  $T_s$ , but no significant impact on the directional anisotropy (less than 0.5 K for the studied cases), which comes to say that radiometric and brightness surface temperature display similar angular variations.

Results of anisotropy are presented in polar plots where concentric circles refer to zenithal viewing angles  $\theta_v$  and radius indicate azimuthal viewing directions  $\varphi_v$ . For  $\theta_v < 48^\circ$  all the  $\varphi_v$  directions can be documented with M740 images. As the area aimed at with the FLIR camera is significantly reduced in relation with backward inclination and smaller FOV, only limited ranges of  $\varphi_v$  angles are investigated for  $\theta_v > 48^\circ$ . This explains the ‘toothed wheel’ aspect of the polar plots presented in that which follows.

It is difficult to provide a precise estimation of the accuracy on the angular TIR variation. The rather good sensitivity of both cameras used (about 0.1 K) and the fact that we consider differential measurements between off-nadir and nadir give us confidence in the variations observed. Among the number of sources of unaccuracy that can be listed (atmospheric corrections, calibration of instruments...), the most critical one probably lies in the natural temporal fluctuations of micrometeorological conditions, wind speed particularly, which may affect the surface temperature differently between flight lines and corresponding viewing directions. We finally estimate a  $\pm 1$  K accuracy on the retrieved angular TIR anisotropy to be realistic.

## 4 RESULTS

### 4.1 Nighttime TIR directional anisotropy

Plate I displays the polar plots of the directional anisotropy for October 4 and February 24 and 25 nights. The anisotropy (difference between oblique and nadir measured surface temperatures) appears to be lower than 1 K for  $\theta_v < 50^\circ$ . No significant variation between azimuthal directions appear. This can be explained by the fact that the distribution of street

directions is rather uniform in the case of Toulouse. For cities displaying a few prevailing directions in the orientation of streets, a possible dependence with azimuthal viewing direction might be expected. A mean dependence of anisotropy with  $\theta_v$  has therefore been derived for each flight by averaging all the  $\varphi_v$  directions. The result (Fig. 8) shows that the 3 nights behave similarly, with anisotropy slightly increasing with zenithal viewing angle. This is due to the fact that nadir viewing measurements are more influenced by horizontal surfaces and roofs, which have the lowest temperature because of radiative losses towards sky. The increasing proportion of walls which are warmer because of energy exchange with other vertical surfaces and building heating explains the corresponding increase in oblique measurements. The swath-like fluctuations that can be observed in Fig. 8 are only artefacts related to the natural temporal variability of temperatures: this makes the nadir reference temperature averaged for each flight line subject to variation between lines, which induces some discontinuities when combining all the information in all directions. This is confirmed (1) by the fact that the amplitude of the fluctuation in Fig. 8 corresponds to half the angular width of the M740 images (about  $30^\circ$ ), and (2) by the linear structures parallel to the flight direction of some discontinuities that can be seen in the polar plots. One may expect anisotropy to be enhanced at the end of the night in relation with stronger cooling of the roofs exposed to clear sky and subject to higher radiative losses than the streets and the walls: it would be interesting to perform measurements at the end of the night closer to dawn to confirm this point.

#### 4.2 Fall/winter daytime TIR directional anisotropy

The polar plots obtained in daytime conditions are also given in plate I. TIR directional anisotropy displays very different patterns between daytime and nighttime.

Daytime plots have been presented in plate I according to increasing UT acquisition times. They all display the same pattern of anisotropy with zenithal viewing angles: anisotropy increases as the hot spot view angle is approached (which corresponds to the exact sun angle with the sun behind). This can be easily explained by the fact that cooler shaded walls are observed when facing the sun, whilst warmer sunlit surfaces are dominant for observations performed with sun from behind. For flights 0441 and 0511, the hot spot clearly appears and is consistent with the sun angle. These results are quite consistent with those obtained in previous experiments over urban canopies. Fig. 9 displays the variation of the anisotropy in the principal solar plane for the 3 flights. Here the zenithal viewing angle is negative (positive) if the urban canopy is observed towards the sun (with the sun behind the viewer). The comparison between the February 24 (0509 flight, despite uncomplete because of small clouds during the first two flight lines) and 25 (0511 flight) dates which have similar meteorological conditions illustrates the increase of the anisotropy throughout the day. Despite the care brought to the intercalibration of the two instruments, residual differences may be observed for some flight lines between the M740 and SC2000 temperature averaged on the overlapping areas in their FOV. For the 0511 flight particularly, they may explain the discontinuity observed at  $\theta_v \sim -40^\circ$  and the possible overestimation of the temperature at the hot spot ( $\theta_v \sim 55^\circ$ ) by about 1.5 K. Nevertheless the overall variation in temperature for the range of zenithal viewing angles investigated is important in the plane aligned with the hot spot (Fig. 9): they reach 4 K (-1 to more than +3 around 9:30 UT for flight 0509), 9 K (between -3 and +6 around 11:00 UT for flight 0441) and 14 K (between -4 and +10 around 14:00UT for flight 0511). The patterns of daytime TIR directional anisotropy are consistent with those observed at the centre of Marseille during the

ESCOMPTE experiment (Lagouarde et al., 2004), with only differences in the angular hot spot position in relation to date and time of measurement.

Fig. 10 displays the variation of TIR directional anisotropy in the perpendicular plane which appears to be much lower than in the principal plane. The sign convention is that negative (positive) zenithal viewing angles correspond to aiming at the canopy towards the left (right) with the sun to one's back. It is important to notice that consequently for  $\theta_v < 0$  the observed walls have been exposed to sun radiation heating for a long time before measurement: conversely for  $\theta_v > 0$  the status of walls has just changed from shaded to sunlit resulting in lower surface temperatures. It is likely that this explains the asymmetry observed in Fig. 10 particularly for 0441 and 0511 flights; the temperatures retrieved for  $\theta_v < 0$  exceed those for  $\theta_v > 0$  by 1 or 2 K. We also notice that the difference between off-nadir and nadir temperatures is positive for the 0509 and 0511 flights, whilst it is negative for the 0441 flight. The reason lies in the fact that the sun elevation is higher during October measurements, which allows the ground to warm whilst it remains shaded and colder than surrounding sunlit walls and roofs in February.

Nighttime anisotropy differs from that in daytime in two ways: (i) by the much lower level of the observed variation ( $\sim 1$  K) and (ii) by a lack of azimuthal influence. This is explained by the fact that the variability of the component temperatures of the elements of the urban canopy seen by the sensor is much larger during daytime (because of the contrast between sunlit and shadowed facets) than during nighttime. It is worth noticing that the acquisition time of night images (around 21:00 or 22:00 UT) is likely to be too late to observe any residual effect of the strong anisotropy observed during the afternoon.: images acquired just after sunset (17:23 and 17:32 UT for October and February dates respectively) or at the beginning of the night would possibly have revealed an anisotropy due to larger west-facing wall temperatures mediated by the thermal inertia of the buildings.

As we are only interested in differences between off-nadir and nadir measurements, the absolute accuracy of the camera is not likely to have a significant impact on the results. The values of the confidence interval on  $\Delta T_s$  estimated as  $2\sigma/n^{1/2}$  ( $\sigma$  and  $n$  standard deviation and number of points for every angular viewing configuration) is always lower than 0.3 K for the sequences we analysed, making all the variations previously reported in this section significant.

### 4.3 Test of a parametric model of TIR directional anisotropy

Practical applications such as correcting angular effects on large swath satellite data for instance require the modelling of the TIR directional signature. We therefore tested the suitability of a parametric hot spot model derived from the one proposed by Roujean (2000) for the optical domain. The difference  $T_s(\theta_v, \varphi_v) - T_{S_{\text{nadir}}}$  between off-nadir and nadir measured surface temperatures here replaces the reflectance and is fitted on the exponential hot spot function as defined by Roujean after several authors, with interception condensed into a  $k$  coefficient (see expressions 14 and 25 in Roujean's paper). For the TIR domain the model can be rewritten as :

$$T_s(\theta_v, \varphi_v) - T_{S_{\text{nadir}}} = (T_{\text{HS}} - T_{S_{\text{nadir}}}) \frac{(e^{-k f} - e^{-k f_N})}{(e^{-k f_{\text{HS}}} - e^{-k f_N})} \quad (1)$$

$$\text{with } f = \sqrt{\tan\theta_s^2 + \tan\theta_v^2 - 2 \tan\theta_s \tan\theta_v \cos\varphi} \quad (2)$$

where  $T_{HS}$  and  $k$  are two parameters corresponding to the surface temperature viewed at hot spot and to a coefficient of interception.  $\theta_S$  is the solar zenith angle and  $\varphi$  the difference between Sun and viewing azimuth angles.  $f_N$  and  $f_{HS}$  are the values of  $f$  function at nadir ( $f_N = \tan\theta_S$ ), and at the hot spot ( $f_{HS} = 0$ ) respectively.

This model was fitted against the dataset assembling all the  $T_s(\theta_v, \varphi_v)$  measurements in the planes comprised between the principal solar plane  $\pm 3^\circ$ . The measured  $T_{S_{nadir}}$  was introduced and the two unknown parameters  $T_{HS}$  and  $k$  determined. In this exercise we considered the brightness temperatures with emissivity equal to unity. As the data of the 0509 flight are prone to possible errors due to light haze above the flight altitude, we only examined the case of the 0441 and 0511 flights. Moreover data from 0511 flight for  $\theta_v < -40^\circ$  were eliminated because of the possible above-mentioned discrepancies in the intercalibration of the two cameras. The results are presented in table II and figure 11. The retrieved  $T_{HS}$  values which provide an indication about the hot spot intensity are consistent with those experimentally observed. The interpretation of the  $k$  coefficient is less easy, but it should be related to the angular position of the hot spot, i.e. the solar zenith angle.

The agreement between the model Eq. (1) and the experimental data is good for the two dates studied. It should obviously be confirmed against other dates. Nevertheless this suggests that the assumptions made which consist in (1) a purely geometrical model, with (2) interception only and no interaction between the different elements within the canopy, remain valid for TIR hot spot modelling to first order. This could provide a guide for the development of future simplified models of the TIR directional anisotropy.

#### 4. CONCLUSION

During the ESCOMPTE 2001 summer experiment over Marseille a methodology was developed for characterizing the TIR directional anisotropy from airborne measurements performed with a TIR camera. A similar protocol was used over the city of Toulouse in the framework of the CAPITOU project. It was slightly improved using 2 cameras (INFRAMETRICS M740 and FLIR SC2000) to extend the zenithal viewing angle up to  $62^\circ$ . The TIR directional anisotropy was investigated in conditions not met in Marseille and the paper presents original results obtained during autumn 2004 and winter 2005, during both daytime and nighttime conditions. Significant directional anisotropy during daytime is confirmed: in the principal plane, and for the range of zenithal viewing angles studied, the variations extend from about -4 K (with the sun in front) up to 10 K (with sun backward). In the perpendicular plane, the variations in directional anisotropy are reduced, but variation from nadir of up to 2 K is observed.

The measurements of anisotropy performed during nighttime (about 5 hours after sunset) over the old city centre of Toulouse in October 2004 and February 2005 revealed limited variations with the zenithal viewing angle only, lower than 2 K in the  $0-62^\circ$  range investigated, and no effect of azimuthal viewing direction. It would be interesting to investigate nighttime TIR anisotropy closer to sunset to evaluate the impact of the thermal inertia of the buildings.

A modelling exercise performed using a simple parametric model on two dates confirmed that, to first order, the TIR directional anisotropy is governed by pure geometrical effects. This justifies the efforts currently undertaken at the laboratory which are based on approaches combining models of surface transfer processes with 3D models to describe TIR directional variations.

Finally the computations have been made considering the entire city centre of Toulouse as the sampling area; the anisotropy results above-presented have therefore been integrated

over about 3 km<sup>2</sup>. The question of the variability in anisotropy over smaller city samples arises, in relation to street orientation or the presence of large squares or buildings for instance. This will have to be studied to define recommendations within the scope of the development of future high spatial resolution TIR sensors.

**Acknowledgements :** The authors thank the SAFIRE group for their contribution to the airborne measurements. They also thank the two reviewers for their useful comments and suggestions. They thank Jean-Louis Roujean (Météo France) for his contribution to the modelling test performed in this paper.

## 5. REFERENCES

- Arnfield A.J. (2003). Two decades of urban climate research: a review of turbulence, exchanges of energy and water, and the urban heat island. *Int. J. Climatology*, 23, 1, 1-26.
- Becker F. & Li S.-L. (1995). Surface temperature and emissivity at various scales: definition, measurement and related problems. *Remote Sens. Rev.*, 12, 225-253.
- Grimmond, C.S.B. & Oke, T.R. (2002). Turbulent Heat Fluxes in Urban Areas: Observations and a Local-Scale Urban Meteorological Parameterization Scheme (LUMPS)', *J. Appl. Meteor.*, 41, 792-810.
- François C., Ottlé C. & Prévot L. (1997). Analytical parameterization of canopy directional emissivity and directional radiance in the thermal infrared. Application on the retrieval of soil and foliage temperatures using two directional measurements. *Int. J. Remote Sens.*, 18 (12), 2587-2621.
- Gastellu-Etchegorry J.P., Martin E., Gascon F. (2004). DART: a 3-D model for simulating satellite images and surface radiation budget. *Int. J. Remote Sens.*, 25 (1): 75-96.
- Guillevic P., Gastellu-etchegorry J.P. Demarty J. et Prévot L. (2003). Thermal infrared radiative transfer within three-dimensional vegetation cover. *J. Geophys. Research - Atmosph.*, Vol. 108 No. D8 10.1029/2002JD002247.
- Lagouarde J-P., Ballans H., Moreau P., Guyon D. & Coraboeuf D. (2000). Experimental study of brightness surface temperature angular variations of Maritime Pine (*Pinus Pinaster*) stands. *Remote Sens. Environ.*, 72, 17-34.
- Lagouarde J-P., Moreau P., Irvine M., Bonnefond J-M., Voogt J., Sollic F. (2004). Airborne experimental measurements of the angular variations in surface temperature over urban areas : case study of Marseille (France). *Remote Sens. Environ.*, 93 (4), 443-462.
- Li X., Strahler A.H. & Friedl M.A. (1999). A conceptual model for effective directional emissivity from nonisothermal surfaces. *IEEE Transactions Geoscience and Remote Sens.*, 37, 5, 2508-2517.
- Martilli A., Clappier A. & Rotach M.W. (2002). An urban surface exchange parameterisation for mesoscale models. *Bound.Layer Meteorol.*, 104, 2, 261-304.
- Masson V. (2000). A physically-based scheme for the urban energy budget in meteorological models. *Bound. Layer Meteorol.*, 94, 357-397.
- Masson, V., Grimmond, C.S.B. & Oke, T.R., (2002). Evaluation of the Town Energy Balance (TEB) scheme with direct measurements from dry districts in two cities. *J. Applied Meteorol.*, 41, 1011-1026.

- Masson V., Gomes L., Pigeon G., Lioussé K., Lagouarde J.-P., Voogt J., Salmond J., Oke T., Legain D., Garrouste O., Lac C., Connan O., and Briottet X. (2007). The Canopy and Aerosol Particles Interactions in Toulouse Urban Layer (CAPITOU) experiment. *Meteorology and Atmospheric Physics*, in this issue.
- Norman J.M. & Becker F. (1995). Terminology in thermal infrared remote sensing of natural surfaces. *Agric. For. Meteorol.*, 77, 153-166.
- Owen T.W., Carlson T.N. & Gillies R.R. (1998). An assessment of satellite remotely-sensed land cover parameters in quantitatively describing the climatic effect of urbanization. *Int. J. Remote Sens.*, 19, 9, 1663-1681.
- Pigeon G., Legain D., Durand P. and V. Masson. 2006. Anthropogenic heat release in an old European city (Toulouse, France). Submitted to *Int. J. of Climatology*.
- Roth M., Oke T.R. & Emery W.J., (1989). Satellite-derived urban heat islands from three coastal cities and the utilization of such data in urban climatology. *Int. J. Remote Sens.*, 10, 11, 1699-1720.
- Roujean J.-L. (2000). A parametric hot spot model for optical remote sensing applications. *Remote Sens. Environ.*, 71, 197-206.
- Sutherland R.A. & Bartholic J.F. (1977). Significance of vegetation in interpreting thermal radiation from a terrestrial surface. *J. Appl. Meteorol.*, 16, (8), 759-763.
- Soux A., Voogt Oke T. (2004). A model to calculate what a remote sensor 'sees' of an urban surface. *Bound. Layer Meteorol.*, 111, 109-132.
- Streukler D.R. (2003). Satellite-measured growth of the urban heat island of Houston, Texas. *Remote Sens. Environ.*, 85, 3, 282-289.
- Sugawara H. & Takamura T. (2006). Longwave radiation flux from an urban canopy: evaluation via measurements of directional radiometric temperature. *Remote Sens. Environ.*, 104, 226-237.
- Vinet, J., 2000: Contribution à la modélisation thermo-aéroluque du microclimat urbain. Caractérisation de l'impact de l'eau et de la végétation sur les conditions de confort en espaces extérieurs. Thèse, Univ. Nantes, 29 nov. 2000, 250pp.
- Voogt J.A. & Oke T.R. (1997). Complete urban surface temperature. *J. Appl. Meteorol.*, 36, 1117-1132.
- Voogt J.A. & Oke T.R. (1998). Effects of urban surface geometry on remotely-sensed surface temperature. *Int. J. Remote Sens.*, 19, 5, 895-920.
- Voogt J.A. & Oke T.R. (2003). Thermal remote sensing of urban climates. *Remote Sens. Environ.*, 86, 370-384.
- Voogt J.A. & Grimmond C.S.B. (2000). Modeling surface sensible heat flux using surface radiative temperatures in a simple urban area. *J. Appl. Meteorol.*, 39, 10, 1679-1699.
- Wang Z., Peng Q., Lu Y. & Jiang Z. (2001). A global infrared image synthesis model for large-scale complex urban scene. *Int. J. of Infrared and Millimeter Waves*, 22, 8, 1193-1208.

## Tables

Flight	Date	Time (UT)		$\varphi_s / \theta_s$	$\varphi_s / \theta_s$
0441	Oct 4, 2004	10:38 – 11:16	morning	159.1 / 51.3	171.4 / 49.5
0443	Oct 4, 2004	22:40 – 23:17	night		
0509	Feb 24, 2005	09:06 – 09:52	morning	130.1 / 67.1	140.1 / 61.3
0510	Feb 24, 2005	21:45 – 22:42	night		
0511	Feb 25, 2005	13:52 – 14:27	afternoon	211.2 / 57.8	220.3 / 61.5
0512	Feb 25, 2005	21:56 – 22:50	night		

**Table I.** Flights performed on October 2004 and February 2005 (UT time) during CAPITOUL experiment IOPs. The variation of azimuthal  $\varphi_s$  (counted positively clockwise from North) and zenithal  $\theta_s$  solar angles during observations are also provided.

Flight	$T_{\text{Snadir}}$	$T_{\text{HS}}$	k	$\theta_s$
0411	26.5	34.9	0.796	49.2
0511	12.1	24.0	0.367	59.8

**Table II.** Fit of the parametric hot spot model of Roujean adapted to TIR domain against experimental airborne data obtained in the principal plane over the city of Toulouse at 2 dates.  $T_{\text{Snadir}}$  and  $\theta_v$  are the nadir brightness surface temperature and solar zenith angle respectively.  $T_{\text{HS}}$  and k are the fitted parameters.

## Figure captions

**Figure 1.** Principle of angular measurements: schematic instrumental setup aboard the aircraft with corresponding areas seen at ground. For a 1500 ft flight height, the approximate size of the areas is 780 x 500 to 600 m and 530 x 200 to 340 m for M740 and SC2000 cameras respectively. The dashed areas indicate the overlapping of the FOV of the 2 cameras and the corresponding area at ground.

**Figure 2.** Protocol of measurements: flight axes. The greyish area represents the studied urban portion. Axes 1 and 1' (principal plane) are first flown beginning with the direction facing the sun (1) indicated by a black circle. The flights along the perpendicular axes (2, 2') follow. The two axes (3, 3') and (4, 4') are then flown at a 45° angle with the principal plane, with a readjustment -see dotted line- to the sun position (white circle) at the later flight time. The greyish trapezoidal shapes schematize the areas at ground corresponding to consecutive images.

**Figure 3.** Aerial photograph of the city centre of Toulouse: 3500x4400 m sample of IGN (Institut Géographique National) panchromatic image of June 24, 1998 (with courtesy of IGN). The white continuous line approximately corresponds to an area of the old city centre for which the structure of the urban canopy has been considered as uniform and which has been taken as the sampling area for extracting TIR directional anisotropy. The circle indicates the position of the central site.

**Figure 4.** Calibration of the FLIR SC2000 TIR. The reference temperature is the temperature of the water thermo-regulated bath.

**Figure 5.** Example of intercalibration of the M740 TIR camera against the SC2000 camera for February 24 flights.

**Figure 6.** Variation of the atmospheric angular correction against the zenithal viewing angle for 0441 flight (daytime). The atmospheric angular contribution is the difference between the atmospheric correction at a given viewing angle and the atmospheric correction at nadir for a same surface temperature  $T_s$  aimed at. It provides an indication of the impact of the atmosphere in the measured directional surface temperature. The range of surface temperatures  $T_s$  for which graphs have been produced are realistic and correspond to the actual conditions met during each flight. A 0.95 value of emissivity has been considered in the calculations.

**Figure 7.** Same as Fig. 6 for 0510 flight (nighttime).

**Figure 8.** Variation of TIR anisotropy with zenithal viewing angle for October 04 (0443) and February 24 (0510) and 25 (0512) night flights.

**Figure 9.** Variation of TIR anisotropy with zenithal viewing angle in the principal plane for October 04 (0441) and February 24 (0509) and 25 (0511) during daytime. The vertical dotted lines allow the reader to situate the zenithal angles corresponding to the respective hot spot positions.

**Figure 10.** Variation of daytime TIR anisotropy with zenithal viewing angle in the perpendicular plane for October 04 and February 24 and 25.

**Figure 11.** Comparison between modelled and measured directional surface temperatures in and around ( $\pm 3^\circ$ ) the principal solar plane for 0441 (a) and 0511(b) flights.

**Plate I.** TIR directional anisotropy experimentally derived from airborne measurements over the city of Toulouse. The difference between oblique and nadir radiative surface temperatures  $T_{S_{\text{off nadir}}} - T_{S_{\text{nadir}}}$  are coded according to colour bars associated to each polar plot. For comparison purpose all the colour scales are identical (-2 to 4 K) for nighttime plots, whilst they have been adapted to each case for daytime to make hot spot clearly visible. The radii of the polar plots correspond to azimuthal viewing directions  $\varphi_v$  and the concentric circles indicate the zenithal viewing angles  $\theta_v$ . Three polar plots are given for nighttime and 3 for daytime (October 4 and February 24 and 25). For daytime the expected positions of the hot spot (i.e. directions aimed at with sun backward)  $\theta_v / \varphi_v$  during each sequence of acquisition (beginning to end) are:  
67.1°/310.1° – 61.3°/320.1° (February 24), 51.3°/339.1° – 49.5°/351.4° (October 4) and 57.8°/31.2° – 61.5°/40.3° (February 25).

### Figures

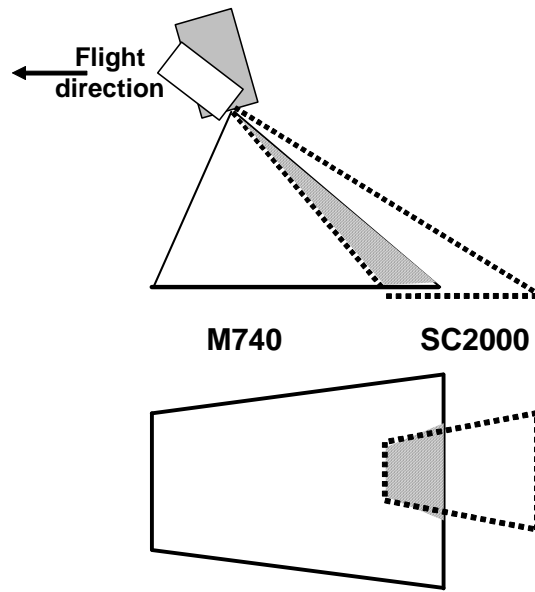


Fig. 1

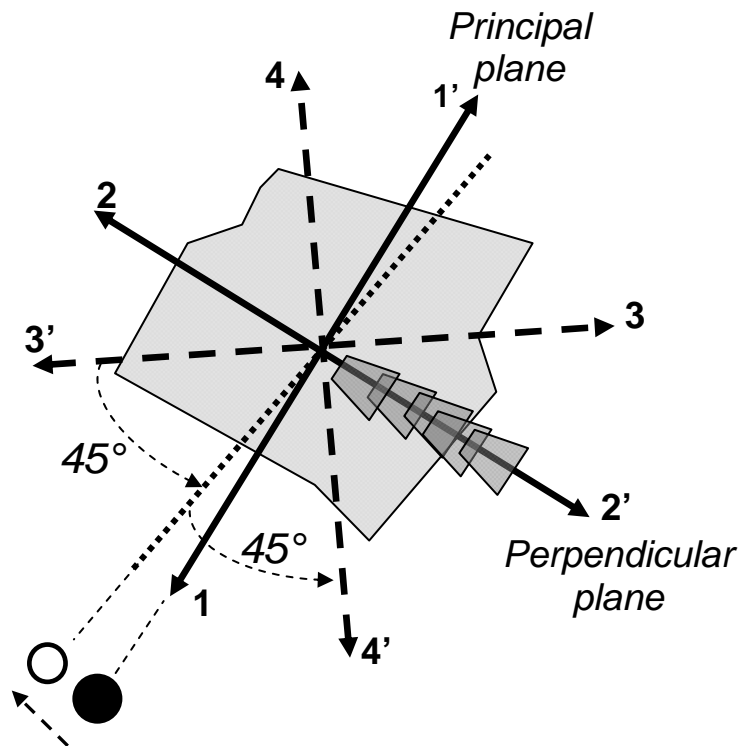


Fig. 2



**Fig. 3**

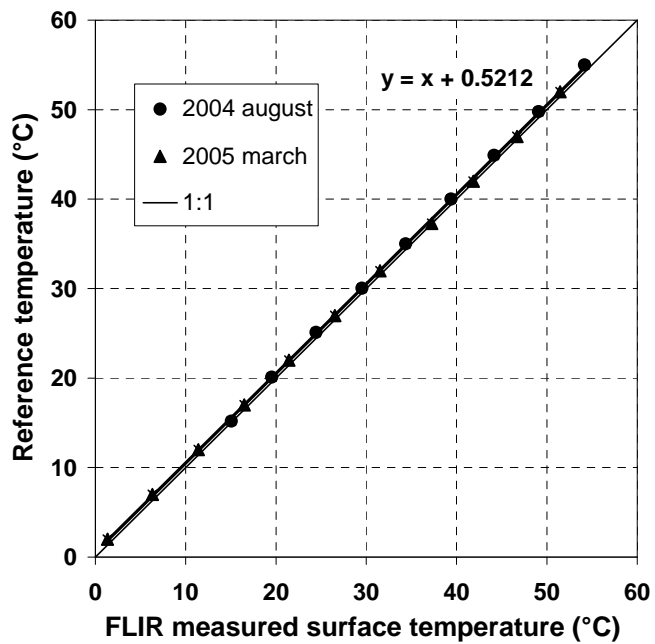


Fig. 4

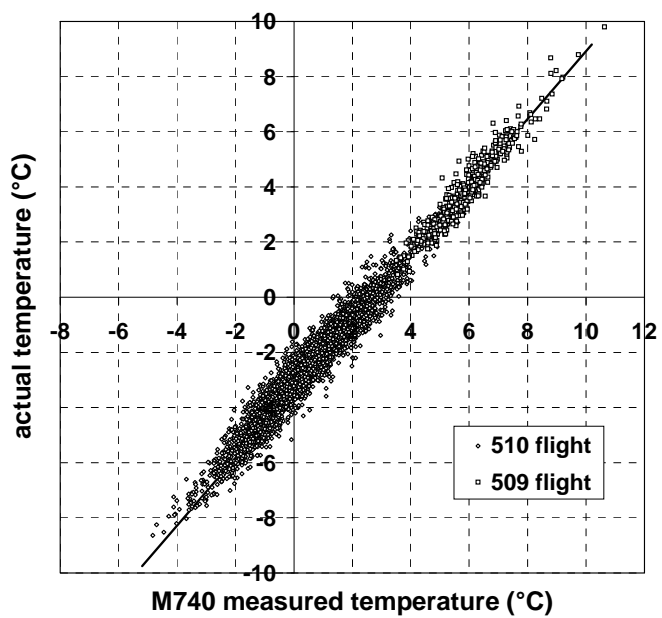


Fig. 5

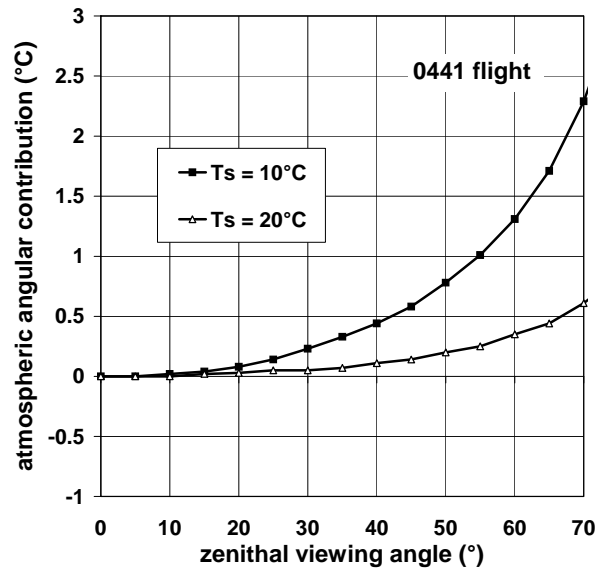


Fig. 6

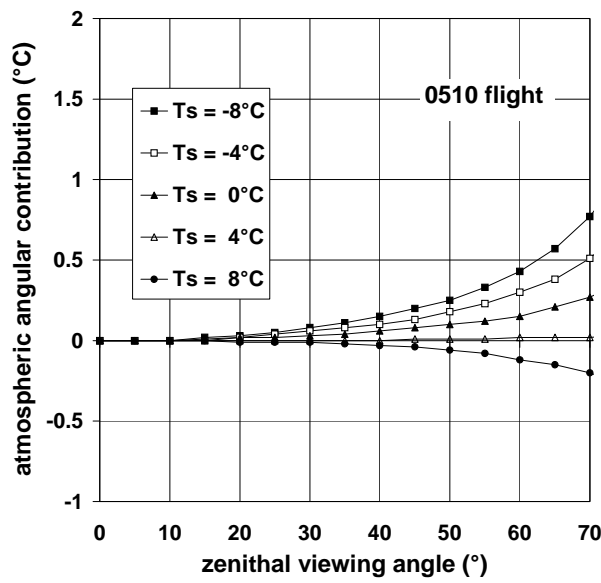


Fig. 7

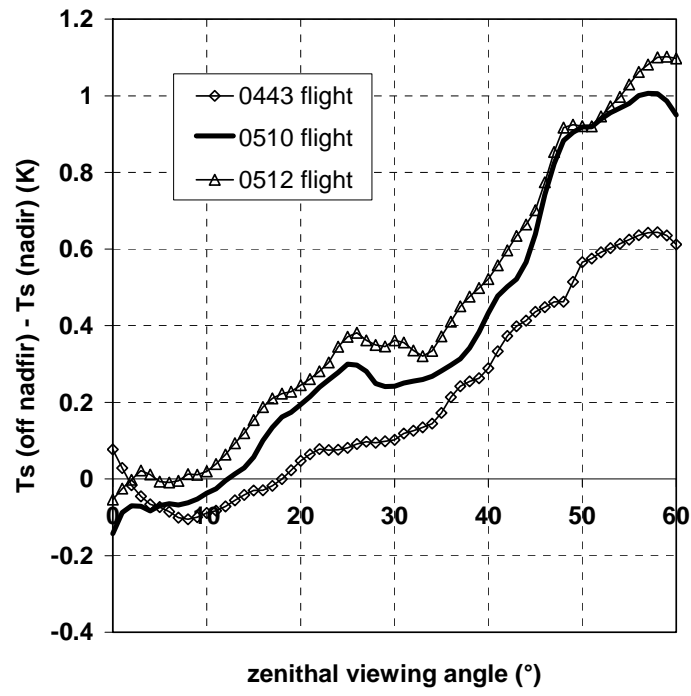


Fig. 8

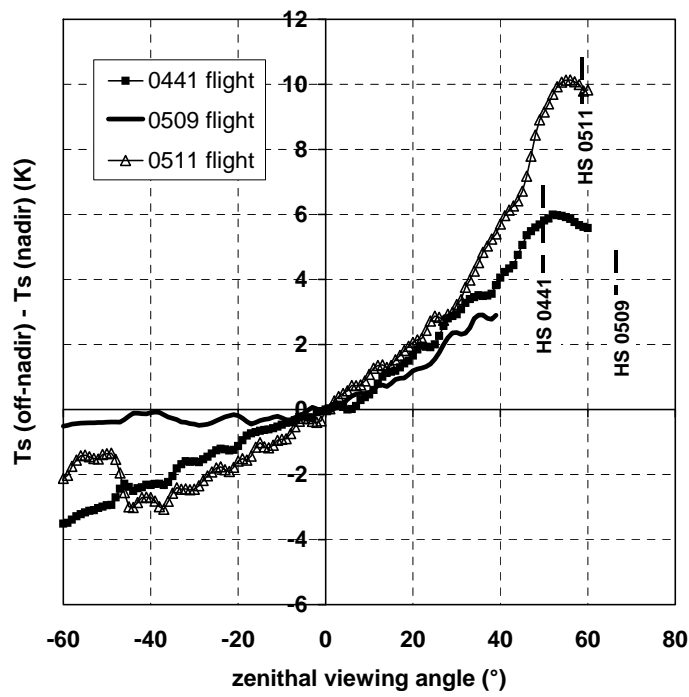


Fig. 9

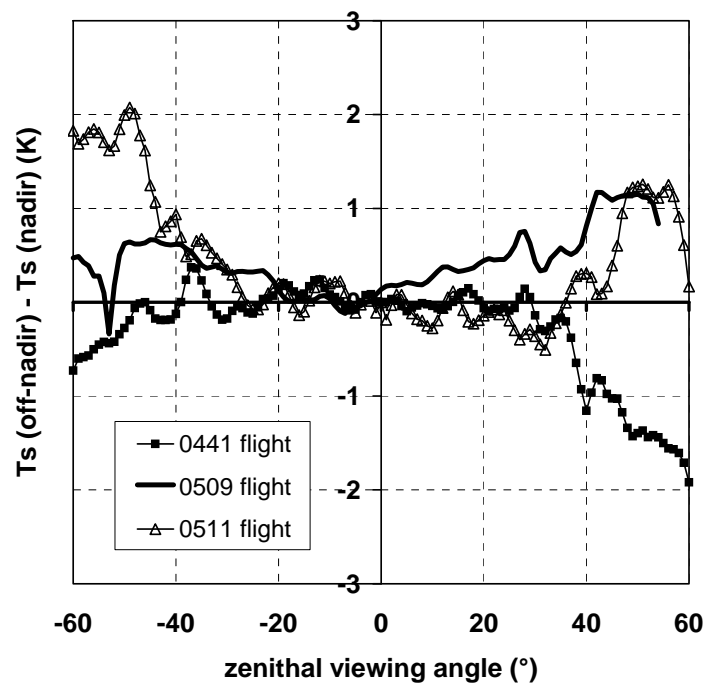


Fig. 10

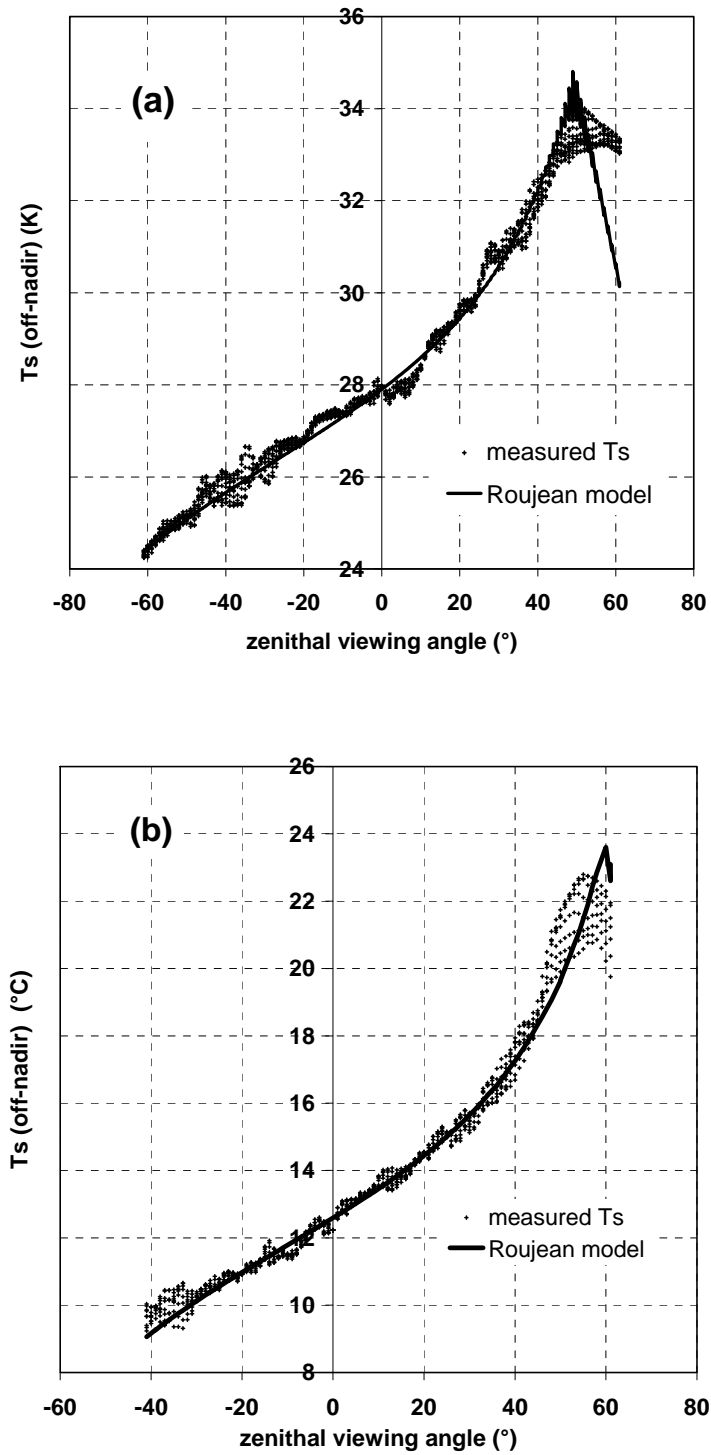


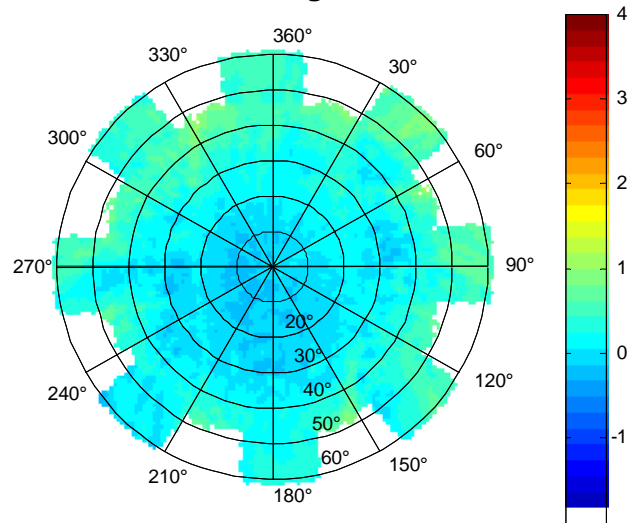
Fig. 11

# Postprint

Version définitive du manuscrit publié dans / Final version of the manuscript published in : **LAGOUARDE J.-P., IRVINE M. Directional anisotropy in thermal infrared measurements over Toulouse city centre during the CAPITOUL measurement campaigns: first results. Meteorology and Atmospheric Physics, numéro spécial CAPITOUL. 19 p.**

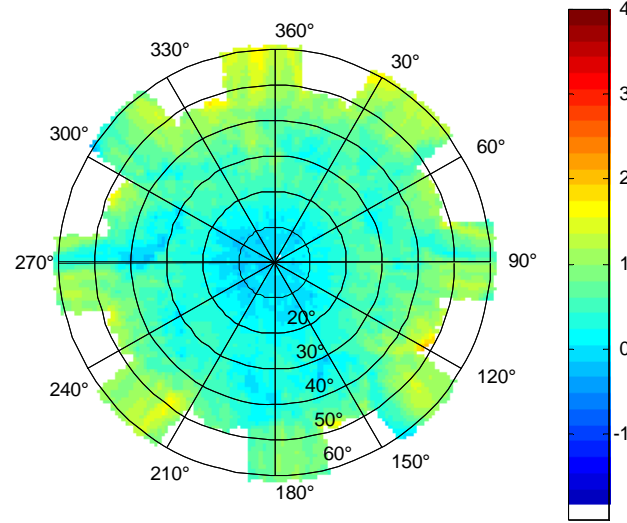
October 04, 2004. 22:40-23:17 UT

0443 flight



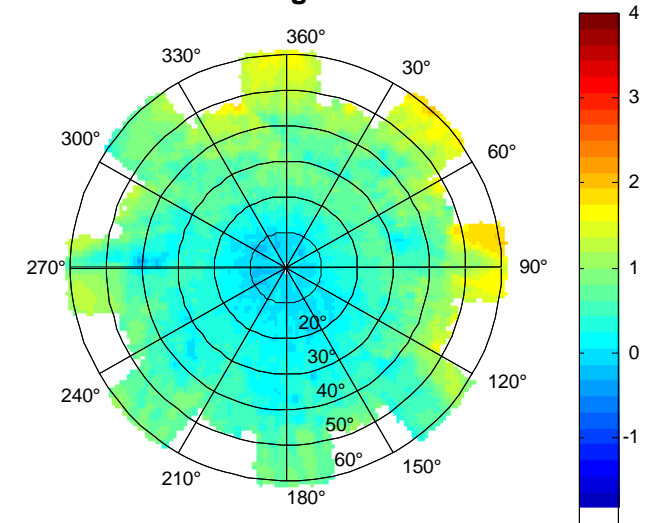
February 24, 2005, 21:45-22:42 UT

0510 flight



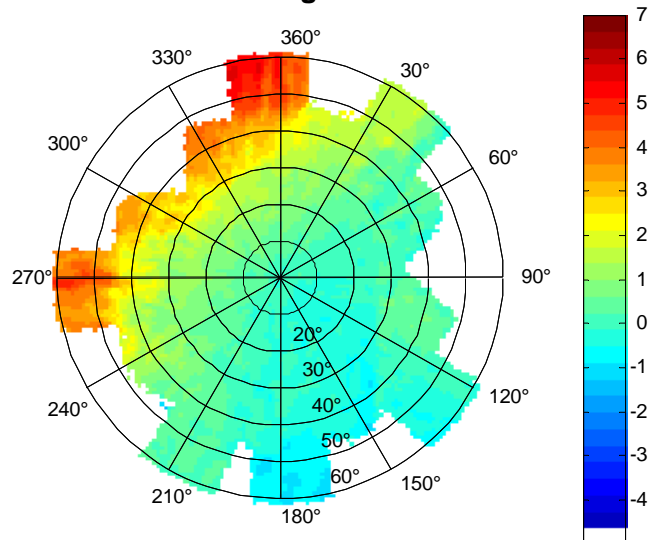
February 25, 2005, 21:56-22:50 UT

0512 flight



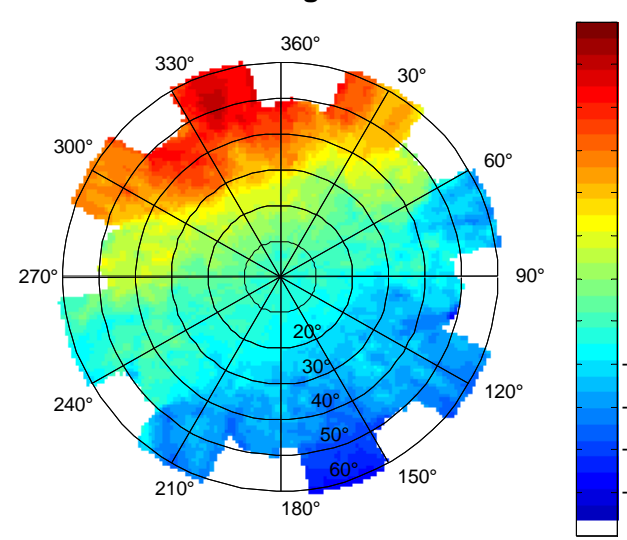
February 24, 2005, 09:06- 09:52 UT

0509 flight



October 04, 2004, 10:38-11:16 UT

0441 flight



February 25, 2005, 13:52-14:27 UT

0511 flight

